RESEARCH ARTICLE

Key Points:
- Strong scintillations on VHF signal are recorded near dip equator, while L-band scintillations are weak
- Near equatorial ionization anomaly (EIA) crest both VHF and L-band scintillations may be moderate to strong
- Model calculations show that equatorial plasma bubble is more structured on the topside of the equatorial F region than near the F peak

Development of intermediate-scale structure at different altitudes within an equatorial plasma bubble: Implications for L-band scintillations

A. Bhattacharyya[1] (ID), B. Kakad[1] (ID), P. Gurram[1], S. Sripathi[1] (ID), and S. Sunda[2]

[1]Indian Institute of Geomagnetism, Navi Mumbai, India, [2]Space Application Centre, Ahmedabad, India

Abstract An important aspect of the development of intermediate-scale length (approximately hundred meters to few kilometers) irregularities in an equatorial plasma bubble (EPB) that has not been considered in the schemes to predict the occurrence pattern of L-band scintillations in low-latitude regions is how these structures develop at different heights within an EPB as it rises in the postsunset equatorial ionosphere due to the growth of the Rayleigh-Taylor instability. Irregularities at different heights over the dip equator map to different latitudes, and their spectrum as well as the background electron density determine the strength of L-band scintillations at different latitudes. In this paper, VHF and L-band scintillations recorded at different latitudes together with theoretical modeling of the scintillations are used to study the implications of this structuring of EPBs on the occurrence and strength of L-band scintillations at different latitudes. Theoretical modeling shows that while S_4 index for scintillations on a VHF signal recorded at an equatorial station may be >1, S_4 index for scintillations on a VHF signal recorded near the crest of the equatorial ionization anomaly (EIA) generally does not exceed the value of 1 because the intermediate-scale irregularity spectrum at F layer peak near the EIA crest is shallower than that found in the equatorial F layer peak. This also explains the latitudinal distribution of L-band scintillations. Thus, it is concluded that there is greater structuring of an EPB on the topside of the equatorial F region than near the equatorial F layer peak.

1. Introduction

Prediction of the strength and latitudinal distribution of ionospheric scintillations on L-band radio signals recorded in low-latitude regions continues to be a challenging problem in view of the role played by these scintillations in degradation of the performance of satellite-based navigation systems. In recent years, several attempts have been made to predict scintillations on VHF and higher-frequency transionospheric radio signals, caused by equatorial spread F (ESF) irregularities [*Retterer*, 2010a, 2010b; *Redmon et al.*, 2010; *Rezende et al.*, 2010; *Carter et al.*, 2014; *de Lima et al.*, 2015]. Focus of the last four of these papers has been on some of the parameters that are at present known to influence the basic condition for the linear growth of the Rayleigh-Taylor (R-T) instability on the bottomside of the postsunset equatorial F region. Some of these parameters also affect the latitudinal distribution of ambient plasma in the low-latitude ionosphere. In their development of a Forecasting Ionospheric Real-time Scintillation Tool, *Redmon et al.* [2010] have found a threshold for the virtual height $h'F$, derived from ground-based ionosonde observations near the geomagnetic equator, for the onset of equatorial VHF/UHF scintillation activity in the Peruvian longitude sector. *Carter et al.* [2014] used Kp values based on solar wind data to drive the National Center for Atmospheric Research Thermosphere-Ionosphere-Electrodynamics General Circulation Model and used the output to compute the flux tube-integrated linear R-T instability growth rate for different apex altitudes of the geomagnetic flux tube above the magnetic equator to predict the occurrence of L-band scintillations at several low-latitude stations in the African and Asian longitude sectors. The paper by *de Lima et al.* [2015] was concerned with predictions of ionospheric scintillations at the magnetic equator using data recorded at the same location. A neural network was trained using a database of 13 predictive attributes, derived from the true height and the vertical drift velocity of the equatorial ionospheric F layer bottomside, values of the $F_{10.7}$ index, and values of the S_4 index, which is the standard deviation of normalized signal intensity fluctuations, to predict the S_4 index on L1 (1.575 GHz) signal from Global Navigation Satellite Systems (GNSS) satellites at a later time on the same day. Aim of the paper by *Rezende et al.* [2010] was to predict L-band scintillations over the Brazilian equatorial ionization anomaly (EIA) region from its previous occurrence at the magnetic equator in the same longitude sector. In this work, data-mining techniques were used

on parameters including ionospheric amplitude scintillation on the GPS L1 signal at the magnetic equator and under the southern crest of the equatorial ionization anomaly EIA, the ionospheric vertical drift velocity over the equator, the geomagnetic index Kp, and $F_{10.7}$. None of these four papers has been concerned with the nonlinear development of the R-T instability over the geomagnetic equator, which gives rise to the intermediate-scale length (approximately hundred meters to few kilometers) structures or irregularities responsible for causing scintillations on transionospheric VHF and higher-frequency radio signals at low-latitude stations.

In a different approach, *Retterer* [2010a, 2010b] has developed a three-dimensional model for the nonlinear evolution of equatorial plasma bubbles (EPBs) as a first step toward obtaining the structure and latitudinal extent of scintillations produced on transionospheric radio signals caused by intermediate-scale length irregularities associated with the EPBs. His model is coupled to a time-dependent model of the ambient ionosphere, so that the background conditions change in response to varying electric fields and neutral winds even as the EPB evolves due to nonlinear growth of the R-T instability. The major drawback of this otherwise fairly realistic model, as far as prediction of scintillations is concerned, is that the spatial resolution (10 km) is inadequate for simulating the generation of intermediate-scale irregularities that produce scintillations on VHF and L-band radio signals. However, an important result that emerged from these 3-D simulations of the EPBs is seen in Figure 2 of *Retterer* [2010b]. This figure shows that the local time evolution of the power spectrum of spatial variations in the magnetic east-west direction of the vertical total electron content (VTEC), down to a scale size of 10 km, is not the same at different geomagnetic latitudes. As discussed in *Bhattacharyya et al.* [2014], these results of *Retterer* [2010b] indicate that prior to 22 h local time (LT), the power spectrum of VTEC fluctuations is shallowest in the EIA crest region at a geomagnetic latitude of ~16°. Since the maximum contribution to VTEC at any location comes from the F layer peak region, it could be concluded that for magnetic east-west scale sizes down to 10 km, the equatorial F layer peak was less structured than that in the EIA crest region prior to 22 LT. It has been shown by *Bhattacharyya et al.* [2001] that on a magnetically quiet day, after ~22 LT, the R-T instability perturbation electric field tends to decay resulting in the descent of the EPBs along with the structures generated within them, with the descending background equatorial F layer. Thus, after 22 LT, field-aligned irregularities on the equatorial topside may not map down to the EIA crest region. Realizing the implications for low-latitude ionospheric scintillations on VHF and L-band radio signals if this pattern of spatial and temporal evolutions of EPB irregularities extended to spatial scales down to 100 m, *Bhattacharyya et al.* [2014] proceeded to study the evolution of irregularities in the intermediate-scale range using data of amplitude scintillations on a 251 MHz signal transmitted from a geostationary satellite and recorded by spaced receivers at an equatorial station. For this purpose, they used the data to derive two parameters: the coherence scale length d_I [*Bhattacharyya et al.*, 2003] and the random velocity V_C [*Bhattacharyya et al.*, 2001] at different stages in the development of the intermediate-scale irregularities. Comparing the results with theoretical computations of d_I, *Bhattacharyya et al.* [2014] concluded that the spectrum of intermediate-scale irregularities in the equatorial F peak region tends to be shallowest after the decay of the perturbation electric fields associated with the R-T instability, a result that could not be obtained from power spectral studies as most of the amplitude scintillation data during the periods under consideration tend to fall in the strong or saturated scintillation category. In future, the recently introduced irregularity parameter estimation technique [*Carrano and Rino*, 2016] may be used to study the evolution of irregularity spectra even in the strong or saturated scintillation regime, using spaced receiver measurements of amplitude scintillations on VHF as well as L-band signals.

Irregularities in the topside equatorial F region map down along geomagnetic field lines to F layer peaks at off-equatorial latitudes that may extend to regions near and even beyond the crest of the EIA. Thus, the results of *Bhattacharyya et al.* [2014] suggested that a shallow intermediate-scale irregularity spectrum on the topside of the equatorial F region would also contribute, along with the higher ambient density present near the EIA crest, to the observation of much stronger L-band scintillations near the crest of the EIA than at the magnetic equator. The suggested latitudinal variation of intermediate-scale irregularity spectrum near the F region peak also has implications for the latitudinal variation of VHF S_4. In this paper, amplitude scintillations on a 251 MHz signal transmitted from a geostationary satellite and recorded at several stations located in the Indian longitude zone have been used together with L-band scintillation data from a network of stations, extending from the geomagnetic equator to a geomagnetic latitude of ~20°N, and theoretical modeling of scintillations on both VHF and L-band frequencies, to establish the nature of the intermediate-scale
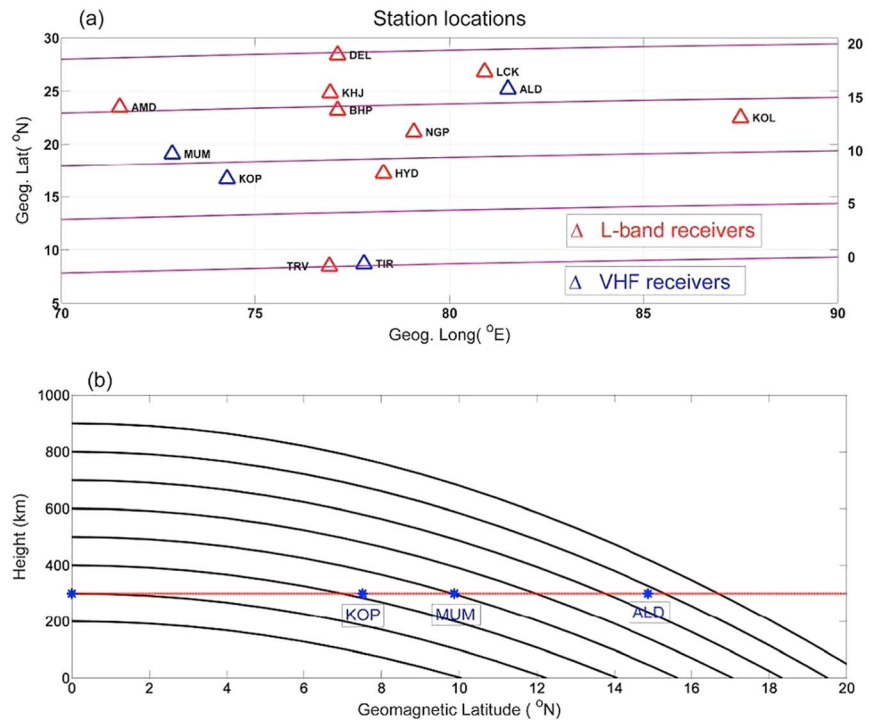
Figure 1. (a) Locations of the stations with VHF and L-band receivers. The mauve lines indicate the geomagnetic latitudes, which are marked on the right-hand side axis. (b) Geomagnetic field lines with different apex altitudes over the geomagnetic equator. Geomagnetic latitudes of the IPPs at an altitude of 300 km for the 251 MHz signal from geostationary satellite UFO2 recorded at the off-equatorial stations KOP, MUM, and ALD are indicated.

irregularity spectrum near the *F* region peak at different geomagnetic latitudes. The results obtained are discussed in the context of 3-D numerical simulations of the evolution of EPBs and in situ observations of structure in EPBs.

2. Latitudinal Variation of VHF and L-Band Amplitude Scintillations

Figure 1a shows the locations of the stations with VHF and L-band receivers, which have provided the data used in this paper. The VHF receivers record amplitude scintillations on a 251 MHz signal transmitted from a geostationary satellite UFO10 located at 72.4°E. The zenith and azimuth (measured eastward from north) angles of the signal paths from UFO10 to the four VHF stations are, respectively, Tirunelveli (TIR): 12° and 212°, Kolhapur (KOP): 19.9° and 190.2°, Mumbai (MUM): 22.4° and 181.4°, and Allahabad (ALD): 31.7° and 202.8°. VHF amplitude scintillations are sampled at intervals of 0.05 s. The geographic and geomagnetic coordinates of the ionospheric penetration points (IPPs) at an altitude of 300 km for the 251 MHz signal from UFO10 to these four stations are listed in Table 1. As EPBs rise to the topside of the equatorial *F* region and develop intermediate-scale structures though nonlinear evolution of the R-T instability initiated on the bottomside of the equator *F* region, the irregularities map down to different latitudes. How high the irregularities have to be over the geomagnetic equator in order to map down to the locations of the IPPs for stations situated away from the geomagnetic equator can be seen from Figure 1b. Data for scintillations

Table 1. Geographic and Geomagnetic Coordinates of the Ionospheric Penetration Points (IPPs) at an Altitude of 300 km for the 251 MHz Signal Paths From UFO10 to the VHF Receiver Locations

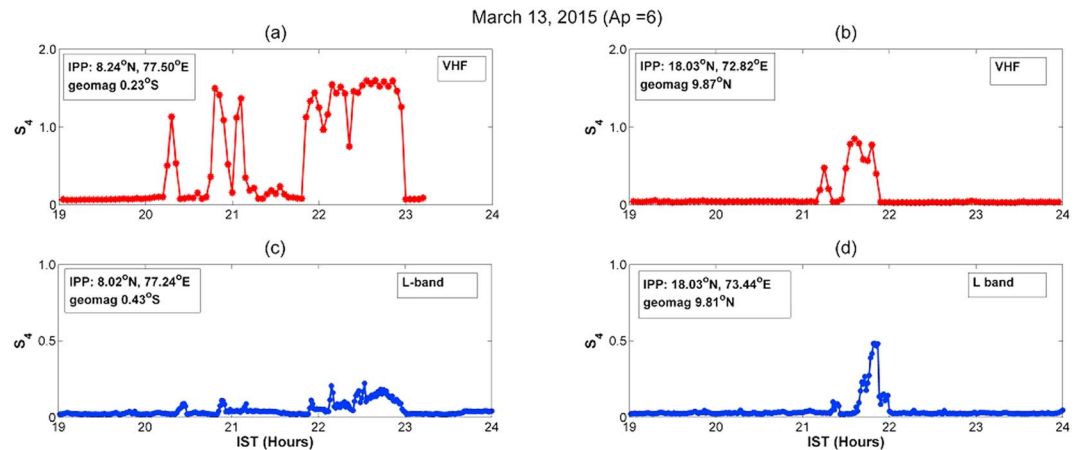| Station	IPP Geographic Latitude	IPP Geographic Longitude	IPP Geomagnetic Latitude	IPP Geomagnetic Longitude
TIR	8.24°N	77.50°E	0.23°S	150.46°E
KOP	15.77°N	74.15°E	7.51°N	147.85°E
MUM	18.03°N	72.82°E	9.87°N	146.78°E
ALD	23.75°N	80.90°E	14.88°N	155.00°E

Figure 2. (a) Variation of S_4 index with time (IST) for the VHF (251 MHz) signal transmitted from geostationary satellite UFO and recorded at equatorial station TIR. (b) Variation of S_4 index with IST for the 251 MHz signal recorded at off-equatorial station MUM located close to the crest of the EIA. (c) Variation of S_4 index with IST for the L1 (1.575 GHz) signal transmitted from geostationary satellite GSAT-10 and recorded at equatorial station TRV close to TIR. (d) Variation of S_4 index with IST for the 1.575 GHz signal recorded at MUM. Geographic coordinates and geomagnetic latitude of the IPPs at 300 km altitude in each case are indicated in the figures. The signal path elevation angles are nearly the same for Figures 2a and 2c and 2b and 2d, respectively, as mentioned in the text.

on an L1 signal (1.575 GHz) are from nine stations, which, with the exception of Nagpur, are part of GPS-Aided Geo-Augmented Navigation (GAGAN), the Indian satellite-based augmentation system network. Raw signal intensity data for L1 sampled at 50 Hz has been used to compute the S_4 index for 1 min intervals. For VHF amplitude scintillations, the S_4 index is computed for 3 min intervals as use of a longer interval for computing VHF S_4 helps in taking into account the wider intensity temporal spectra on VHF as compared to L-band.

On 13 March 2015, which was a magnetically quiet day ($\Sigma Kp = 11-$, $Ap = 6$), data from a GNSS receiver located at Mumbai (MUM), where a VHF receiver is also located, was available. On this day, saturated scintillations with S_4 exceeding 1 were recorded between 20 and 23 Indian standard time (IST) $=$ UT $+$ 5.5 h) on the 251 MHz signal received at Tirunelveli (TIR) near the geomagnetic equator, as shown in Figure 2a. Strong amplitude scintillations, with S_4 reaching a value close to 0.9, were recorded between 21 and 22 IST on the 251 MHz signal received at MUM, as seen in Figure 2b. Scintillations were also recorded on a L1 (1.575 GHz) signal transmitted from the geostationary satellite GSAT-10 (PRN 128) located at 83°E and received at MUM and at the equatorial station Trivandrum (TRV) located close to TIR.

The S_4 values on L1 recorded at TRV and MUM during the night of 13 March 2015 are plotted as a function of IST in Figures 2c and 2d. The signal path elevation angles for the VHF and L1 signals received at TIR and TRV, respectively, are 78° and 77.8°. Coordinates of the IPP at an altitude of 300 km for these signals are VHF: 8.24°N, 77.5°E; geomagnetic 0.23°S and L1: 8.02°N, 77.24°E; geomagnetic 0.43°S. Thus, both the VHF and L1 signals are traversing nearly the same region of irregularities at about the same elevation angle. This can also be seen from the similarity in the patterns of temporal variation of S_4 on VHF and L1 signals in Figures 2a and 2c, although the magnitudes of S_4 are very different. This layer of irregularities is producing scintillations with $S_4 > 1$ on the VHF signal while giving rise to only very weak scintillations on L1 with S_4 rarely exceeding 0.2. For weak scintillations produced by EPB irregularities, which are highly elongated in the direction of the geomagnetic field and hence may be considered to be essentially two dimensional, with a power law irregularity spectrum of the form $\Phi_{\Delta N}(q) \propto q^{-m}$, the S_4 index is expected to show a signal frequency (f) dependence of the form: $S_4 \propto f^{-n}$, where $n = (m + 3)/4$ [Yeh and Liu, 1982; Bhattacharyya et al., 1990]. However, in the present case, S_4 on the 251 MHz signal exceeds 1, where the signal frequency dependence of S_4 departs significantly from the weak scintillation case. The signal path elevation angles for the VHF and L1 signals received at MUM are 67.6° and 65°, respectively. Coordinates of the IPP at an altitude of 300 km for these signals are VHF: 18.03°N, 72.82°E; geomagnetic 9.87°N and L1: 18.03°N, 73.44°E; geomagnetic 9.81°N. Thus, here also both the VHF and L1 signals are traversing nearly the same region of irregularities at about the same elevation angle. This layer of irregularities is producing moderate to strong scintillations on the VHF signal with $S_4 \sim 0.9$, while on
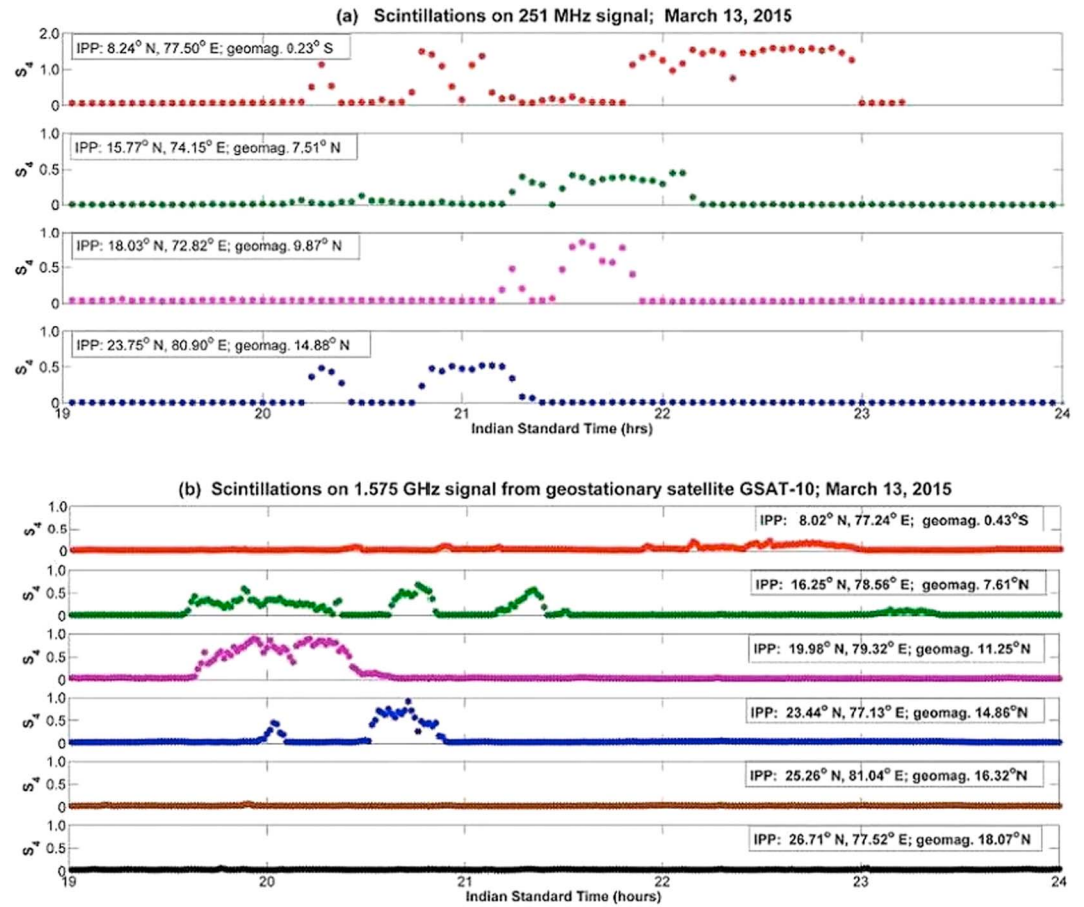
Figure 3. (a) Variation of S_4 index with IST for scintillations on the 251 MHz signal transmitted from geostationary satellite UFO and recorded at all four VHF receiver stations on 13 March 2015. (b) Variation of S_4 index with IST for scintillations on the 1.575 GHz signal transmitted from geostationary satellite GSAT-10 and recorded at L-band receiver stations for which the signal path elevation angle was not less than 55°.

L1 the scintillations are somewhat weaker with S_4 not exceeding 0.5 as can be seen in Figures 2b and 2d. Thus, while the VHF S_4 at MUM is much less than that at the equatorial location, the irregularities located at a geomagnetic latitude ~10°N, which are producing scintillations on the VHF signal recorded at MUM, are giving rise to much stronger scintillations on the L1 signal than the irregularities that are causing scintillations on the signals recorded at the equatorial locations.

Plots of S_4 for scintillations on the 251 MHz signal recorded at all the four VHF receiver stations on 13 March 2015 are shown in Figure 3a. S_4 indices computed for scintillations on a 1.575 GHz signal transmitted from the geostationary satellite GSAT-10 and recorded at L-band receiver stations for which the signal path elevation angle was at least 55° are also plotted as a function of IST in Figure 3b. Locations of the IPPs at an altitude of 300 km along with the geomagnetic latitude of the IPPs are mentioned in the figures. No L-band scintillations are recorded for IPPs with geomagnetic latitudes greater than ~15°. It is seen from Figure 3a that for the VHF receivers at KOP and MUM, the signal IPPs, which are at geomagnetic latitudes of 7.51°N and 9.87°N, are located to the west of the VHF signal IPPs for the stations TIR and ALD, which are at geomagnetic latitudes of 0.23°S and 14.88°N, respectively. Thus, the VHF scintillations recorded between ~20:15 and 21:15 IST at the equatorial location TIR and at ALD, which is north of MUM, were produced by irregularities generated shortly after sunset, and which drifted eastward, and did not encounter the VHF signals to KOP and MUM. There is no counterpart of the VHF scintillations recorded at TIR staring at about 21:50 IST, at ALD probably because the perturbation electric field associated with the R-T instability had largely decayed by that time [*Bhattacharyya et al.*, 2001] so that the irregularities moved downward with the ambient plasma over the magnetic equator, and no longer mapped onto the *F* region over ALD. The irregularities that produce VHF
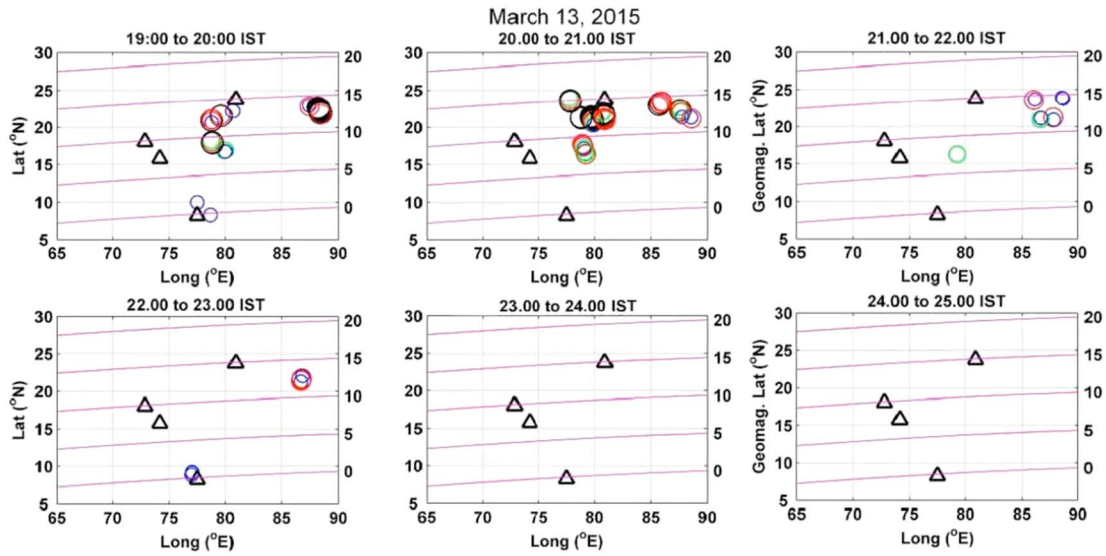
Figure 4. Spatial and temporal variations of L-band scintillations recorded for all visible GNSS satellites during periods when the signal path elevation angle was not less than 55°. Five-minute averages of L-band S_4 index are plotted along the tracks of IPPs at 300 km altitude for each satellite as circles of different colors and sizes to represent the level of S_4. Four different levels of S_4 are shown: (1) blue circles for $0.15 \leq S_4 \leq 0.25$, (2) green circles for $0.25 \leq S_4 \leq 0.35$, (3) red circles for $0.35 \leq S_4 \leq 0.5$, and (4) black circles for $S_4 > 0.5$. The triangles mark the locations of the IPPs at 300 km altitude for the VHF signal recorded at the four VHF stations. The mauve lines indicate the geomagnetic latitudes, which are marked on the right-hand side axis.

scintillations recorded at KOP and MUM are generated over the magnetic equator to the west of TIR at a later time, and as they drift eastward they may be linked with the irregularities that give rise to VHF scintillations recorded at TIR starting at about 21:50 IST. The irregularities over the magnetic equator were at a height lower than 800 km required to map down to 300 km over ALD but still were at a height of at least 500 km to map down to 300 km over MUM. The required eastward drift speed of the irregularities is ~135 m/s.

It is to be noted that while the S_4 index for VHF scintillations recorded at TIR exceeded 1 for most of the periods with scintillations, this did not happen at the other stations with higher geomagnetic latitudes and lower elevation angles of the signal paths. S_4 for VHF scintillations recorded at MUM approached a value of 1, but that for KOP was lower. As already noted L-band scintillations recorded at the equatorial station were the weakest, while it is seen from Figure 3b that those for L-band signal IPP at a geomagnetic latitude of 11.25° were the strongest. Irregularities that produce moderate and strong L-band scintillations during ~19:35–20:30 IST, on signals with IPPs at geomagnetic latitudes of 7.61°N and 11.25°N, respectively, are generated over the geomagnetic equator to the east of the VHF stations TIR, KOP, and MUM and drift eastward so that they are not associated with the irregularities that produce VHF scintillations recorded at TIR, KOP, and MUM. They also do not seem to extend to 800 km over the geomagnetic equator to map down to the F region above ALD as they drift through a longitude of 80.9°E.

To see the effect of the dynamics of the irregularities on L-band scintillations, the spatial and temporal distributions of L-band scintillations recorded for all the other visible GNSS satellites during periods when the signal path elevation angle was not below 55° are shown in Figure 4. For better clarity, in each case, 5 min averages of L-band S_4 have been plotted along the tracks of IPPs at 300 km altitude for each visible satellite with signal path elevation angle $\geq$55°. It is seen from these plots that on this day presence of ionospheric irregularities that produce scintillations on an L1 signal is restricted to geomagnetic latitudes $\leq$15°. Between 19 and 20 IST, irregularities in the 75–80°E longitude band are freshly generated, which move eastward, intensify, and extend up to a geomagnetic latitude of 15°. Strong L-band scintillations with $S_4 > 0.5$ are associated with IPPs in geomagnetic latitude range of 10–15° during the period of 20–21 IST. However, no L-band scintillations with $S_4 \geq 0.15$ are recorded near the geomagnetic equator. On this night, L-band scintillations are not recorded at the stations considered after 23 IST. In earlier studies, the absence of significant L-band scintillations near the geomagnetic equator when strong L-band scintillations were observed around the crest of the EIA was attributed to the higher ambient plasma density around the crest of the EIA [*Mullen et al.*, 1985; *Groves et al.*, 1997; *Bhattacharyya et al.*, 2003; *Sripathi et al.*, 2008; *Whalen*, 2009;

Nishioka et al., 2011]. However, this does not explain the latitudinal variation in VHF S_4 seen in Figure 3a. *Hajra et al.* [2012], who have studied the occurrence of VHF and L-band scintillations in the region of the EIA crest at 88°E, have also not reported VHF S_4 exceeding 1 at these latitudes. In order to understand the latitudinal characteristics of S_4 for both the VHF and L1 signals, theoretical calculation of the S_4 index for a 251 MHz and a 1.575 GHz signals propagating through irregularity layers with different characteristics is carried out in the next section.

3. Model Calculation of S_4 Index

Computation of S_4 for 251 MHz and 1.575 GHz signals propagating through ESF irregularities, which is based on a statistical description of the irregularities, requires characterization of the spectrum of intermediate-scale length (approximately hundred meters to few kilometers) irregularities in terms of some parameters and solving the equation satisfied by the fourth moment of the complex amplitude of the incident radio wave as it propagates through the irregularity layer followed by free space to reach the ground receiver. Wavelengths of 251 MHz and 1.575 GHz radio signals are 119.5 cm and 19 cm, respectively. These wavelengths are much shorter than the scale sizes of intermediate-scale irregularities. Therefore, when these radio signals travel through the irregularity layer, they propagate essentially along the line of sight with very little deviation. Thus, the phenomenon of ionospheric scintillation involves forward scattering; i.e., the incident wave is scattered within a small angular cone around the direction of propagation of the radio wave [*Yeh and Liu*, 1982]. Since the irregularities are aligned with the geomagnetic field, intensity in the ground scintillation pattern produced by the scattering changes only in the magnetic east-west direction. Hence, the ESF irregularities may be considered to be essentially two dimensional in a theoretical calculation of S_4. The x axis is taken to be in the magnetic east-west direction, and the signal propagates along the z direction. Initially, a plane wave of unit amplitude is considered to be incident on the irregularity layer of thickness L along the z direction. As the wave propagates through the irregularity layer, phase and amplitude fluctuations build up and the wave acquires a complex amplitude $u(x, z)$, which is a function of x and z coordinates. The fourth moment of the complex amplitude is defined as

$$\Gamma_4(x_1, x_2, x_3, x_4, z) = \langle u(x_1, z) u(x_2, z) u^*(x_3, z) u^*(x_4, z) \rangle \tag{1}$$

and it satisfies the equation [*Yeh and Liu*, 1982]:

$$\frac{\partial \Gamma_4}{\partial \zeta} = \left[-i \frac{\partial^2}{\partial \xi_1 \partial \xi_2} - \frac{1}{2\zeta_L} F(\xi_1, \xi_2) \right] \Gamma_4 \tag{2}$$

$F(\xi_1, \xi_2)$ is determined by the irregularity characteristics, and is 0 outside the irregularity layer. $\xi = q_0 x$ and $\zeta = q_0^2 z / k$ are the normalized x and z coordinates, where $q_0 = 2\pi/R_0$, R_0 being the outer scale of the irregularity spectrum, and $k = 2\pi/\lambda$, λ being the signal wavelength. Thus, $\zeta_L = q_0^2 L / k$ is the normalized thickness of the irregularity layer. S_4 index for the signal is computed from

$$S_4^2 = \frac{\langle I^2 \rangle - \langle I \rangle^2}{\langle I \rangle^2} = \frac{1}{I_0^2} \Gamma_4(0, 0, \zeta_R) - 1 \tag{3}$$

where $I_0 = 1$ for an incident wave of unit amplitude and $\zeta_R = q_0^2 z_R / k$, z_R being the distance of the receiver from the top of the irregularity layer, which is taken to be at $z = 0$. A general spectrum for the density fluctuations, introduced by *Shkarofsky* [1968] to characterize power law irregularity spectra with slope $-m$, with the following form in the two-dimensional case, is used here:

$$\Phi_{\Delta N}(q) = \frac{\sigma_{\Delta N}^2 (q_0 r_0)^{\frac{m-2}{2}} r_0^2}{2\pi K_{\frac{m-2}{2}}(q_0 r_0)} \left(r_0 \sqrt{q_0^2 + q^2} \right)^{-\frac{m}{2}} K_{\frac{m}{2}}\left(r_0 \sqrt{q_0^2 + q^2} \right) \tag{4}$$

where $\sigma_{\Delta N}$ is the standard deviation of the density fluctuations and represents the strength of the irregularities, r_0 is the inner scale of the irregularity spectrum, and K_n is the modified Bessel function of the second kind of order n. For $r_0 \ll R_0$, $q \gg q_0$, and $r_0 q \ll 1$, a power law irregularity spectrum is obtained: $\Phi_{\Delta N}(q) \propto q^{-m}$. The relationship between $F(\xi_1, \xi_2)$ and $\Phi_{\Delta N}(q)$ and a description of the split-step method used to solve equation (2) are given in *Bhattacharyya and Yeh* [1988] and *Engavale and Bhattacharyya* [2005].

S_4 indices computed for an incident radio signal of frequency 251 MHz, and four different slopes—m for a power law irregularity spectrum, are plotted in Figure 5a as functions of the standard deviation of normalized
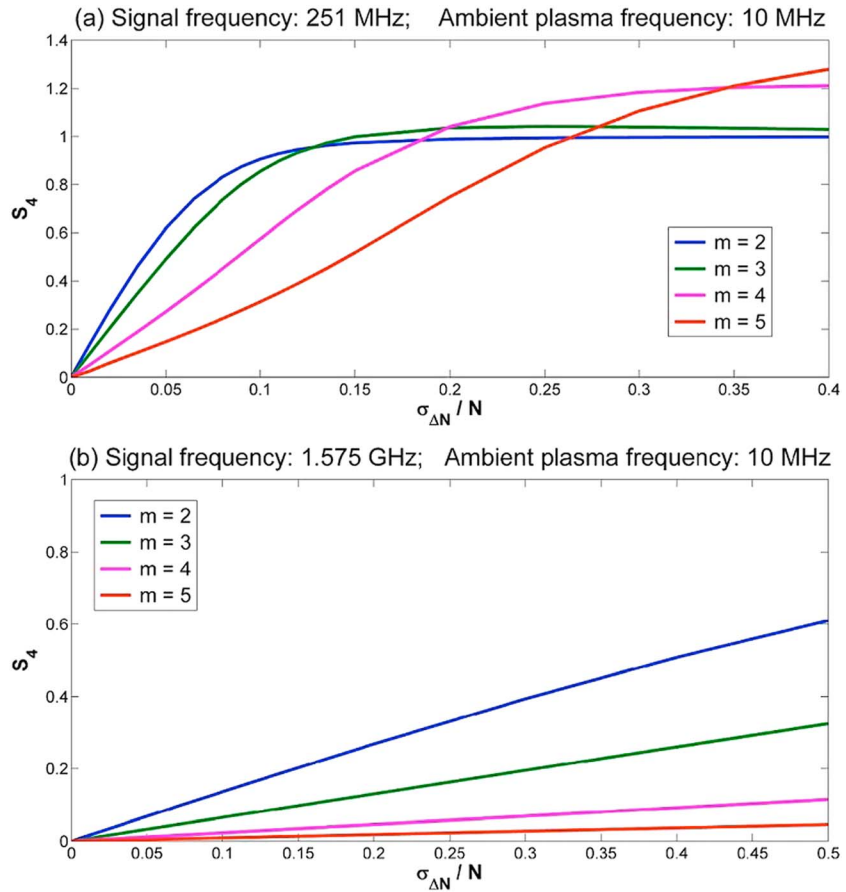
Figure 5. (a) S_4 indices computed for an incident radio signal of frequency 251 MHz as a function of the standard deviation of normalized electron density fluctuations, N being the ambient plasma density. The irregularities are characterized by a power law irregularity spectrum with slope m. Four values of m are considered, keeping other irregularity parameters the same. (b) Same as in Figure 5a for a signal of frequency 1.575 GHz.

density fluctuations, $\sigma_{\Delta N}/N$, where N is the background density. For this figure, N is constant and corresponds to an ambient plasma frequency of 10 MHz. It is to be noted that S_4 is determined by $\sigma_{\Delta N}$, but normalized density fluctuations are used in the plots as density fluctuations are generally described as a percentage of the ambient density. For a higher ambient density, the same percentage fluctuation would imply a higher $\sigma_{\Delta N}$, and the figure would shift toward the left. Values of other model parameters used in the computation of S_4 are $r_0 = 10$ m, $R_0 = 10$ km, $z_R = 350$ km, and $L = 50$ km. Thus, the irregularities in the intermediate-scale range have a power law spectrum. It is seen from Figure 5a that whereas for $m = 2$, S_4 reaches a saturation value of 1 with increasing $\sigma_{\Delta N}$ without exceeding one, the maximum values of S_4 are greater than 1 for the steeper irregularity spectra, with the highest S_4 values obtained for $m = 5$. Using a power law phase screen model, *Rino* [1979] had obtained asymptotic expressions for S_4 valid under very strong scattering conditions, which showed that for a one-dimensional phase screen, which corresponds to $L \to 0$ in our 2-D model, the S_4 index asymptotically approaches unity for $1 < m < 3$, while the limiting value of S_4 exceeds 1 for $m \geq 3$. This has been attributed to strong focusing of the signal by irregularities with steeper spectra when small-scale structures which are more effective in scattering the radio waves, and thereby destroy the focusing effects of the large-scale irregularities, are absent. In the present study, only irregularity spectra with a single slope have been considered and the inner and outer scales have not been varied. In a recent paper, *Carrano and Rino* [2016] have considered a two-component power law irregularity spectra, with slopes m_1 and m_2, in a calculation of scintillation statistics. Their numerical results demonstrate that in the limit of asymptotically strong scatter, the S_4 index is controlled entirely by the high-frequency portion of the irregularity spectrum, when the irregularity spectra are shallow ($m_1 \leq m_2 < 3$), while it is determined by the low-frequency portion of the irregularity spectrum when the irregularity spectra are steep ($m_2 > m_1 > 3$). Thus, in the case of a
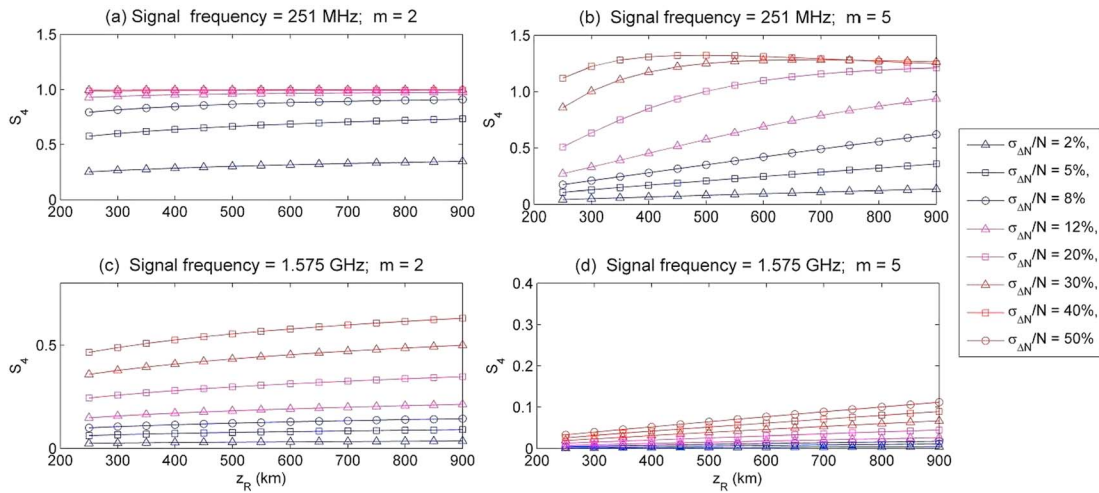
Figure 6. (a) S_4 index computed as a function of the distance of the top of the irregularity layer from the receiver for an incident radio signal of frequency 251 MHz and power law irregularity spectrum with slope −2. The standard deviation of normalized electron density fluctuations is varied from 2% to 50% keeping other irregularity parameters the same. (b) Same as in Figure 6a but for a power law irregularity spectrum with slope −5. (c) Same as in Figure 6a but for an incident radio signal of frequency 1.575 GHz. (d) Same as in Figure 6b but for an incident radio signal of frequency 1.575 GHz.

single-component spectrum considered here, the S_4 index depends on the outer scale only for the steep irregularity spectra. The S_4 index may attain even higher values for $m > 3$ than shown in Figure 5a if a larger outer scale is used and the irregularities are sufficiently strong because with increasing m the maximum value of S_4 is reached at a higher value of $\sigma_{\Delta N}/N$. Results for the shallow spectrum (m =2) are insensitive to the outer scale. It is to be noted that the asymptotic results of *Carrano and Rino* [2016] are applicable only to saturated scintillations, which are not uncommon for the VHF signal. Scintillations on L-band are far less likely to saturate, and therefore, the results of *Carrano and Rino* [2016] would not generally be applicable to them.

In Figure 5b, S_4 indices computed for an incident radio signal of frequency 1.575 GHz are plotted as functions of $\sigma_{\Delta N}/N$ for single-component power law irregularity spectra with the same slopes as in Figure 5a. As expected, the highest S_4 indices are obtained for m =2. For $m > 3$ scintillations are very weak with $S_4 < 0.15$. Height of the postsunset equatorial F layer is highly variable [*Basu et al.*, 2009; *Fejer*, 2011], and therefore, model calculations have also been carried out for different values of z_R for a shallow irregularity spectrum with m =2 and a steep irregularity spectrum with m =5, keeping the other parameters r_0, R_0, and L the same as for Figures 5a and 5b. The results for two signal frequencies: 251 MHz and 1.575 GHz, are shown in Figure 6, where in each subplot S_4 is plotted as a function of z_R for density fluctuation levels in the irregularities varying from 2 to 50% of the ambient density, which is taken to correspond to a plasma frequency of 10 MHz as in the case of Figures 5a and 5b. In a phase screen approximation, varying z_R would imply changing the Fresnel scale. It is seen from Figure 6 that for a shallow irregularity spectrum varying z_R has no effect on S_4 in the strong scattering regime, with S_4 asymptotically approaching a value of 1 as the irregularity strength is increased. For weak scintillations produced by irregularities with a power law spectrum, increasing the effective Fresnel scale is expected to increase S_4 as is seen in Figures 6c and 6d, which are for a signal of frequency 1.575 GHz. However, for strong irregularities with a steep spectrum a higher z_R up to 500 km is more favorable for producing an $S_4 > 1$ on the VHF signal as can be gauged from Figure 6b. It is also to be noted from Figures 5 and 6 that an increase in background density does not result in substantially increasing the strength of scintillations on L-band if the irregularity spectrum is steep. L-band S_4 index increases much more rapidly with increasing irregularity strength when the irregularity spectrum is shallow.

Maximum contribution to ionospheric scintillations recorded at any location is from irregularities around the F peak traversed by the signal, where the ambient density is maximum. Comparison of VHF and L-band S_4 indices obtained at the two equatorial locations TIR and TRV, shown in Figures 2a and 2c, respectively, with the model calculation results, indicates that around the equatorial F peak region, the irregularity spectrum must be steep. For producing VHF and L-band scintillations recorded at MUM shown in Figures 2b and 2d, irregularities over the geomagnetic equator at this longitude must be at an altitude of 500 km in order to
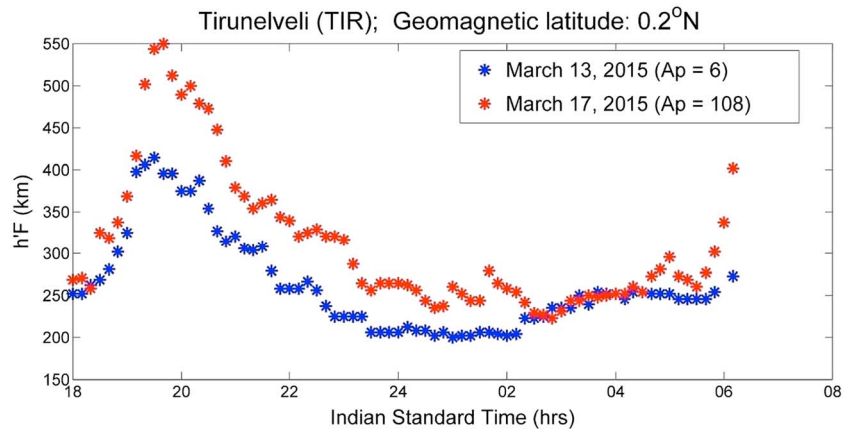
Figure 7. Virtual height of the *F* layer at the equatorial station TIR on the magnetically quiet night of 13–14 March 2015 and on the night of 17–18 March 2015, which was magnetically disturbed.

map down to an altitude of 300 km near the IPPs at geomagnetic latitudes of 9.87°N and 9.81°N, respectively. Comparison of VHF and L-band S_4 indices obtained at MUM on 13 March 2015 in the light of the model calculation results shown in Figures 5a and 5b leads to a scenario where the irregularities near the *F* peak at about 10° geomagnetic latitude must have a shallow spectrum. Therefore, it may be concluded that irregularities at an altitude of about 500 km at the magnetic equator have a shallower spectrum than the irregularity spectrum near the equatorial *F* peak. This picture of the evolution of intermediate-scale irregularities within an EPB at different heights above the geomagnetic equator would explain the near absence of L-band scintillations near the geomagnetic equator when moderate to strong L-band scintillations are observed between geomagnetic latitudes of 10–15°. In order to investigate the role played by background conditions on the evolution of intermediate-scale irregularities within an EPB at different heights over the geomagnetic equator, VHF and L-band scintillation data for a magnetically disturbed day are considered in the next section.

4. Structuring of EPB on a Magnetically Disturbed Night

VHF and L-band scintillations recorded at the various stations on the night of 17 March 2015 are considered because a major geomagnetic storm occurred on this day, with *Dst* reaching a minimum of −228 nT, $\Sigma Kp = 48$, and $Ap = 108$. There was prompt penetration of a large eastward electric field of magnetospheric origin, possibly modified by disturbance dynamo effects, into the equatorial ionosphere in the Indian longitude region, around the time of normal prereversal enhancement (PRE) of the eastward electric field. This resulted in an increase of *h'F* to as high as ~550 km over the equatorial station TIR [*Ramsingh et al.*, 2015; *Kakad et al.*, 2016] so that the conditions that prevailed in the equatorial ionosphere on this night are significantly different from those that existed on the night of 13 March 2015. For comparison, *h'F* obtained from a digital ionosonde located at TIR for these two nights are plotted in Figure 7. The promptly penetrated eastward electric field around dusk added to the postsunset PRE eastward electric field in the equatorial ionosphere caused *h'F* at TIR on 17 March 2015 to be raised by ~150 km around 20 IST compared to *h'F* on 13 March 2015. This resulted in faster development of EPBs in the *F* region over TIR [*Basu et al.*, 2007; *Kakad et al.*, 2016], the EPBs extended to greater altitudes over the geomagnetic equator and as a result mapped down to higher latitudes. This can be seen from Figure 8, where plots of S_4 for scintillations on the 251 MHz signal recorded at all the four VHF receiver stations on 17 March 2015, and for scintillations on a 1.575 GHz signal transmitted from the geostationary satellite GSAT-10 and recorded at L-band receiver stations for which the signal path elevation angle was at least 55°, are shown as a function of IST in Figures 8a and 8b. Locations of the IPPs at an altitude of 300 km along with the geomagnetic latitude of the IPPs are mentioned in the figures. Figure 8a shows that S_4 for the VHF signal recorded at TIR with IPP at geomagnetic latitude of 0.23°S is mostly >1 before midnight decreasing below 1 in the postmidnight hours, while S_4 for the VHF signal recorded at MUM with IPP at geomagnetic latitude of 9.87°N is ~1 up to 22:30 IST but does not exceed 1. As on 13 March, this is higher than S_4 for the VHF signals recorded at KOP and ALD with IPPs
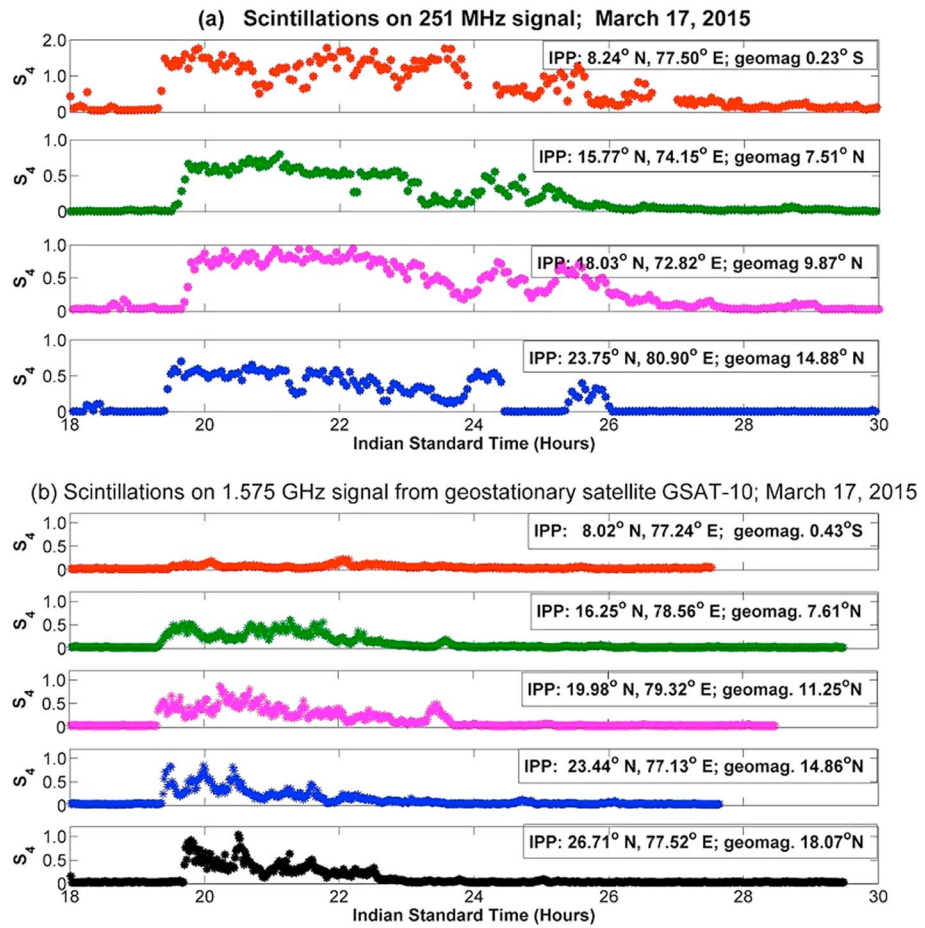
Figure 8. Same as in Figure 3 for 17–18 March 2015.

located at geomagnetic latitudes of 7.51°N and 14.88°N. It is seen from Figure 8b that on 17 March 2015, while strong scintillations are recorded on the L1 signal from GSAT-10 at geomagnetic latitudes between ~11 and 18°N, once again, almost no scintillations are found on the L1 signal recorded at the equatorial station TRV. Also, L-band scintillations on the GSAT-10 signal received at the four stations located between 7.6 and 18.1°N geomagnetic latitude do not extend beyond midnight.

Spatial and temporal distributions of L-band scintillations recorded for all the other visible GNSS satellites on 17 March 2015 during periods when the signal path elevation angle was not below 55°are shown in Figure 9. As shown in Figure 4, 5 min averages of L-band S_4 have been plotted along the tracks of IPPs at 300 km altitude for each visible satellite with signal path elevation angle ≥55°. On this night, strong L-band scintillations are produced by intermediate-scale irregularities that are present near the F peak between geomagnetic latitudes of 10 to 20°N. They are also observed in a wider longitude band than on March 13. EPBs have to reach a height of ~1100 km above the geomagnetic equator in order that irregularities map down to an altitude of 300 km at a geomagnetic latitude of 20°. Thus, a difference of ~150 km in the postsunset height rise of the equatorial F layer on 13 and 17 March has resulted in the EPBs reaching a maximum height above the geomagnetic equator on the night of 17 March, which is ~300 km higher than that on 13 March 2015. Therefore, the altitude of the postsunset equatorial F layer is an important factor not only in the occurrence of EPBs, which has been established in earlier studies [*Sultan*, 1996; *Fejer et al.*, 1999; *Valladares et al.*, 2004], but also in the altitudinal extent of the EPBs and development of intermediate-scale structure at different heights within an EPB.

5. Discussion and Conclusions

Power spectra of weak amplitude scintillations have a power law form: $P(\nu) \propto \nu^{-m}$ for frequencies ν greater than the Fresnel frequency when they are produced by irregularities with a power law spectrum. For weak
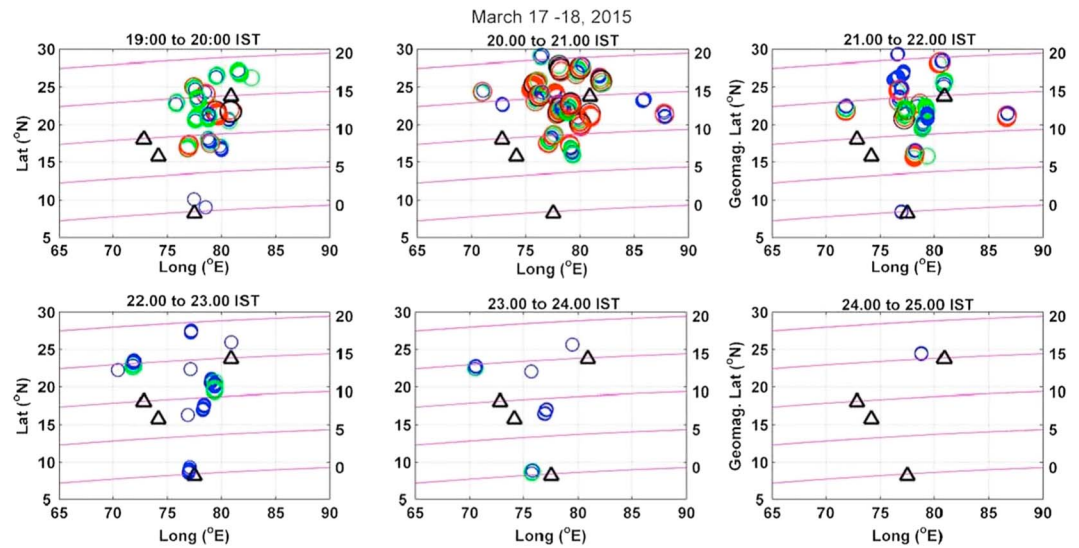
Figure 9. Same as in Figure 4 for 17–18 March 2015.

scintillations, spatial scales in the irregularities are directly related to temporal scales in the ground scintillation data through an effective drift speed V with which the ground scintillation pattern moves past a receiver. This drift speed converts spatial scales in the ground scintillation pattern into temporal scales in the data recorded by the receiver [*Yeh and Liu*, 1982]. Thus, for weak amplitude scintillations, the spectral index m is determined by the spectral index of the irregularity spatial power law spectrum. However, as the irregularity strength increases, multiple scattering and focusing of the radio signals come into play, and the relationship between irregularity and scintillation spectra is no longer straightforward [*Booker and MajidiAhi*, 1981; *Forte*, 2008; *Carrano and Rino*, 2016]. Weak scintillations produced by nighttime equatorial F region irregularities generally occur for a short duration in the beginning of a scintillation event, when irregularities are still developing, and for a longer duration toward the end of a scintillation event, during the decay phase of irregularities [*Bhattacharyya and Rastogi*, 1985; *Kakad et al.*, 2012]. As the EPB rises to the topside through nonlinear evolution of the R-T instability, absence of significant ion-neutral collisions on the topside and also reduced coupling of the topside with the conjugate E regions helps the shorter-scale structures to grow there before they develop near the F region peak [*Huba et al.*, 1985; *Bhattacharyya*, 2004]. Thus, at the beginning of a VHF scintillation event, intermediate-scale irregularities that produce only weak scintillations on a VHF signal may be located on the topside, where the ambient plasma density is low and hence the irregularities are weak. Later when irregularities of east-west scale size ~1 km start to develop near the equatorial F region peak, these irregularities produce very strong VHF scintillations because of the much higher ambient plasma density present there. Results presented in this paper and the earlier paper by *Bhattacharyya et al.* [2014] show that by this time, irregularities of scale sizes of a few hundred meters also develop on the topside but are yet to form near the equatorial F region peak. As a result the intermediate-scale irregularity spectrum is much steeper near the equatorial F region peak than on the topside, which explains the occurrence of very strong VHF scintillations but very weak or no L-band scintillations produced by the equatorial ionospheric irregularities.

As seen in section 3, very strong kilometer-scale irregularities with a steep irregularity spectrum give rise to focusing of the VHF radio signal yielding S_4 indices >1. In the month of March 2015, VHF scintillation events were recorded at the equatorial station TIR with S_4 >1 during some part of the night on 23 nights, while for the same VHF signal recorded at MUM, which is located close to the crest of the EIA, S_4 indices close to 1 were observed during those events, but S_4 did not exceed 1 [*Kakad et al.*, 2016]. This indicated that the spectrum of irregularities that mapped down from an altitude of 500 km above the geomagnetic equator to the IPP for MUM at 300 km altitude must have a shallow spectrum compared to the spectrum of irregularities near the equatorial F peak. Theoretical computation of S_4 indices on 251 MHz and 1.575 GHz signals propagating through a layer of irregularities with power law spectra with varying slopes has shown that while irregularities with a steep spectrum are capable of producing S_4 >1 on the VHF signal, they give rise to very weak

scintillations on the L1 signal. At the same time, a shallow slope of the irregularity spectrum does not allow S_4 to exceed 1 on the VHF signal but gives rise to much stronger scintillations on the L1 signal as compared to irregularities with steep spectra. This scenario explains the observations of VHF and L-band scintillations not only at the equatorial stations and MUM shown in Figure 2 but also at a chain of stations extending up to 20° in geomagnetic latitude. More importantly, theoretical calculation of S_4 also shows that the strong L-band scintillations observed near the EIA crest cannot arise only due to the much higher ambient density that exists at the F peak in this region. Unless the irregularities have a relatively shallow slope, generally, a higher ambient plasma density cannot play an important role in producing strong L-band scintillations. However, during the solar maximum period in 2000–2002, L-band scintillations with $S_4 > 1$ have been observed at Ascension Island near the EIA crest [*Bhattacharyya et al.*, 2003; *Carrano and Rino*, 2016]. This demonstrates that in the presence of very high ambient plasma density in the EIA crest region, irregularities with a steep spectrum may also be strong enough to produce scintillations on L-band with $S_4 > 1$. A steep irregularity spectrum in the EIA region during solar maximum conditions indicates that the topside equatorial F region irregularities may not have evolved in an inertial regime because of the higher ambient neutral density giving rise to higher ion-neutral collision frequencies at these altitudes.

It is to be noted that equatorial and low-latitude scintillations in the Indian region are significantly stronger during the vernal equinox compared to the autumn equinox [*Sripathi et al.*, 2011]. Even during vernal equinox, there may be days when S_4 does not exceed 1 at an equatorial station. This does not imply that the irregularity slope near the equatorial F peak is less steep on these days, but it is an indication of the irregularities not being strong enough. This is clearly brought out by the evolution of the coherence-scale or dominant-scale size in the ground scintillation pattern studied in the earlier paper [*Bhattacharyya et al.*, 2014], where all the seasons were considered. Focus of the present paper is on the implications of the variation of the irregularity spectrum with altitude over the magnetic equator for the latitudinal distribution of L-band scintillations.

At present, numerical simulations of the development of structures in three-dimensional EPBs, as they rise to the topside in the equatorial ionosphere due to nonlinear evolution of the R-T instability in the postsunset equatorial ionosphere, do not have adequate spatial resolution to yield the irregularity spectrum in the intermediate-scale range [*Retterer*, 2010a; *Yokoyama et al.*, 2014]. Development of 3-D models for EPBs or plumes was carried out by *Retterer* [2010a, 2010b] with the aim of predicting the latitudinal distribution of scintillations on UHF and L-band signals. However, as noted in section 1, the magnetic east-west spatial resolution of his models was limited to 10 km. Thus, the simulation was not suitable for prediction of scintillations on UHF and L-band signals. The interesting result that emerged from the study of *Retterer* [2010b], as discussed in detail in section 1, is that in early stages of development of irregularities within EPBs, before 22 LT, the ionosphere around equatorial F layer peak is less structured than that near the F layer peak in the EIA crest region. After 22 LT, due to the decay of the R-T instability perturbation electric field on a magnetically quiet day [*Bhattacharyya et al.*, 2001], the EPB and associated irregularities move downward along with the background F layer over the geomagnetic equator. Thus, the spectrum of VTEC fluctuations at the geomagnetic equator becomes shallower than that before 22 LT. However, after 22 T, the equatorial irregularities also become weaker on account of a lower ambient density, although the irregularities near the equatorial F peak may have a shallower spectrum compared to earlier times. The results obtained in the present paper show that this picture of the evolution of the irregularity spectrum at different heights above the geomagnetic equator is true down to intermediate-scale structures, which produce scintillations on VHF and higher-frequency transionospheric radio signals, and therefore, it is necessary to take this aspect into consideration for proper prediction of the latitudinal distribution of scintillations produced by EPBs. Without recognizing this factor, it is not possible to fully explain the occurrence of very weak L-band scintillations near the geomagnetic equator when strong L-band scintillations are observed near the EIA crest.

The high-resolution bubble model developed by *Yokoyama et al.* [2014] has a spatial resolution of ~1 km and does not cover the intermediate-scale range. However, this model also clearly shows that as an EPB grows nonlinearly from the crest of a large-scale wave structure upwelling, it bifurcates at the top and subsequently the topside of the equatorial F region becomes more structured or turbulent. Features of the three-dimensional plasma density distribution of the fully developed EPB displayed in their Figure 4 clearly show that at an altitude of 300 km, the EPB has much shorter-scale-length east-west structure at a geomagnetic latitude of 15° than near the geomagnetic equator, where the irregularity spectrum would be much steeper.

This simulation result also supports the conclusions derived from the present study of the latitudinal distribution of VHF and L-band scintillations. For better prediction of VHF and L-band scintillations, in addition to improved spatial resolution, simulations of EPB evolution must also investigate how ambient topside conditions such as the topside plasma density distribution affect the development of structure in EPBs. In the past, using a 2-D model of the EPB, *Sekar and Raghavarao* [1995] had shown that the upward drift of the plasma bubbles has a significant dependence on the fractional depletion that involves the ambient topside electron density distribution. This in turn plays a role in the zonal and vertical extents of the EPB. It is expected that the reduced ion-neutral collision frequency as well as reduced coupling of the topside with the conjugate *E* regions may also affect the structuring of EPBs on the topside [*Huba et al.*, 1985; *Bhattacharyya*, 2004]. These factors need to be explored in future 3-D model simulations of EPB development.

In situ observations of EPBs also yield important information about the nature of irregularity spectra at different geomagnetic latitudes and hence at different apex altitudes over the geomagnetic equator. *Shume and Hysell* [2004] carried out a spectral analysis of plasma drift data from AE-E satellite during its passage through strong spread *F* irregularities. Fluctuations in plasma drift are proportional to the electric field fluctuations associated with the R-T instability, which map along geomagnetic field lines from the equatorial ionosphere to higher geomagnetic latitudes. Data analyzed by *Shume and Hysell* [2004] pertained to irregularities that were mapped from the topside equatorial *F* region along geomagnetic field lines with apex heights of ~600–900 km. Their analysis yielded a one-dimensional spectral slope close to −5/3 for irregularities of scale sizes ranging from about 1 to 100 km. This indicated that these irregularities were in an inertial regime. The instrument noise floor prevented the extension of their results below 1 km. In situ high-resolution ion density data from the low-inclination C/NOFS satellite have been used to derive the spectral slope of intermediate-scale range irregularities [*Rodrigues et al.*, 2009], which was found to be ≈−5/3. These results came from the rather low altitude of ~450 km, where irregularities are not expected to be in an inertial regime. The authors attributed their results to the unusually low neutral densities under the prevailing extended solar minimum conditions, so that ion-neutral collision frequencies at this altitude were much lower than usual, resulting in an inertial regime. Another set of in situ observations of EPB structures involved the analysis of variations of the magnetic field component parallel to the main geomagnetic field, measured by a fluxgate magnetometer on board the Challenging Mini-satellite Payload during the years 2000–2005 [*Xiong et al.*, 2012; *Lühr et al.*, 2014]. Electron density variations are well correlated with fluctuations in the parallel component of the geomagnetic field on account of the diamagnetic effect. The shortest scales considered by *Xiong et al.* [2012], which were in the range of 15–76 km, were found to have maximum occurrence on geomagnetic flux tubes with an apex height of about 800 km at all longitudes. Occurrence rate of these structures was also found to decrease after 22 LT. *Lühr et al.* [2014] found the occurrence rate of intermediate-scale events to be symmetrically distributed about the geomagnetic equator with peak occurrence at geomagnetic latitudes of 10–15°. Since the ambient density is lower at the geomagnetic equator, they found the amplitudes of magnetic field fluctuations to be lower than the resolution of their measurements. Hence, these authors were unable to obtain the irregularity spectrum near the geomagnetic equator, but their results for higher geomagnetic latitudes show the tendency of the irregularity spectra to be shallower at higher geomagnetic latitudes. All these in situ observations support the picture of the development of structure within the EPBs suggested in the present paper in order to explain the latitudinal distribution of VHF and L-band scintillations.

In summary, in the present paper an effort has been made to explain why the S_4 index for amplitude scintillations on a VHF signal recorded at a station close to the EIA crest does not generally exceed 1 even when accompanied by moderate to strong scintillations on an L-band signal recorded there, while scintillations on an L-band signal recorded at an equatorial station are either absent or very weak ($S_{4L} \leq 0.2$) even when a VHF signal recorded there has strong scintillations with $S_{4\,VHF} > 1$. These observations are explained by theoretical computations of S_4 for incident radio signals of frequencies 251 MHz and 1.575 GHz propagating through a layer of irregularities with power law spectra with different spectral slopes. Results show that for $S_{4\,VHF}$ to exceed 1, the irregularity spectrum must have a steep slope so that the incident signal may be focused by the larger-scale irregularities. This does not happen when the irregularity spectrum is shallow because the shorter-scale irregularities scatter the incident radio wave. The theoretical results also show that this scenario is able to explain the absence of L-band scintillations when the irregularity spectrum is steep. The observed amplitude scintillations are an integrated effect with maximum contribution at any latitude

coming from the region around the F peak at that latitude. It is also seen from the theoretical results that an increased electron density in the F peak region at the EIA crest would not cause moderate to strong L-band scintillations unless the irregularity spectrum there is sufficiently shallow. Thus, the results obtained in this paper show that around the equatorial F peak region, the irregularity spectrum is much steeper than in the topside of the equatorial F region, which maps down to higher latitudes, thus producing $S_4 > 1$ on a VHF signal and very weak scintillations on L-band signal recorded in the equatorial region. This situation persists before the perturbation electric field associated with the R-T instability disappears. After that the topside equatorial irregularities come down with the ambient plasma but are now weaker in strength, although they have a shallow spectrum. This scenario is supported by 3-D simulations of the development of structure in EPBs at scales larger than the intermediate scales required to produce scintillations. In situ observations made so far also support the conclusions of this paper. Observational and theoretical results reported in the present paper provide evidence that intermediate-scale length irregularities in EPBs, which include Fresnel-scale irregularities that produce scintillations on VHF and L-band signals, are mapped from the topside of the equatorial F region to the EIA crest region. Hence, for better prediction of low-latitude L-band scintillations, it is necessary to identify the ambient conditions that play a role in the development of EPB structure on the topside of the nighttime equatorial ionosphere.

References

Basu, S., S. Basu, F. J. Rich, K. M. Groves, E. MacKenzie, C. Coker, Y. Sahai, P. R. Fagundes, and F. Becker-Guedes (2007), Response of the equatorial ionosphere at dusk to penetration electric fields during intense magnetic storms, *J. Geophys. Res.*, 112, A08308, doi:10.1029/2006JA012192.

Basu, S., S. Basu, J. Huba, J. Krall, S. E. McDonald, J. J. Makela, E. S. Miller, S. Ray, and K. Groves (2009), Day-to-day variability of the equatorial ionization anomaly and scintillations at dusk observed by GUVI and modeling by SAMI3, *J. Geophys. Res.*, 114, A04302, doi:10.1029/2008JA013899.

Bhattacharyya, A. (2004), Role of E region conductivity in the development of equatorial ionospheric plasma bubbles, *Geophys. Res. Lett.*, 31, L06806, doi:10.1029/2003GL018960.

Bhattacharyya, A., and K. C. Yeh (1988), Intensity correlation function for waves of different frequencies propagating through a random medium, *Radio Sci.*, 23, 791–808, doi:10.1029/RS023i005p00791.

Bhattacharyya, A., and R. G. Rastogi (1985), Amplitude scintillations during the early and late phases of evolution of irregularities in the nighttime equatorial ionosphere, *Radio Sci.*, 20(4), 935–946, doi:10.1029/RS020i004p00935.

Bhattacharyya, A., R. G. Rastogi, and K. C. Yeh (1990), Signal frequency dependence of ionospheric amplitude scintillations, *Radio Sci.*, 25, 289–297, doi:10.1029/RS025i004p00289.

Bhattacharyya, A., S. Basu, K. M. Groves, C. E. Valladares, and R. Sheehan (2001), Dynamics of equatorial F region irregularities from spaced receiver scintillation observations, *Geophys. Res. Lett.*, 28(1), 119–122, doi:10.1029/2000GL012288.

Bhattacharyya, A., K. M. Groves, S. Basu, H. Kuenzler, C. E. Valladares, and R. Sheehan (2003), L-band scintillation activity and space-time structure of low-latitude UHF scintillations, *Radio Sci.*, 38(1), 1004, doi:10.1029/2002RS002711.

Bhattacharyya, A., B. Kakad, S. Sripathi, K. Jeeva, and K. U. Nair (2014), Development of intermediate scale structure near the peak of the F region within an equatorial plasma bubble, *J. Geophys. Res. Space Physics*, 119, 3066–3076, doi:10.1002/2013JA019619.

Booker, H., and G. MajidiAhi (1981), Theory of refractive scattering in scintillation phenomena, *J. Atmos. Sol. Terr. Phys.*, 43, 1199–1204, doi:10.1016/0021-9169(81)90035-0.

Carrano, C. S., and C. L. Rino (2016), A theory of scintillation for two-component power law irregularity spectra: Overview and numerical results, *Radio Sci.*, 51, 789–813, doi:10.1002/2015RS005903.

Carter, B. A., et al. (2014), Using solar wind data to predict daily GPS scintillation occurrence in the African and Asian low-latitude regions, *Geophys. Res. Lett.*, 41, 8176–8184, doi:10.1002/2014GL062203.

de Lima, G. R. T., S. Stephany, E. R. de Paula, I. S. Batista, and M. A. Abdu (2015), Prediction of the level of ionospheric scintillation at equatorial latitudes in Brazil using a neural network, *Space Weather*, 13, 446–457, doi:10.1002/2015SW001182.

Engavale, B., and A. Bhattacharyya (2005), Spatial correlation function of intensity variations in the ground scintillation pattern produced by equatorial spread F irregularities, *Indian J. Radio Space Phys.*, 34, 23–32.

Fejer, B. G. (2011), Low latitude ionospheric electrodynamics, *Space Sci. Rev.*, 158(1), 145–166, doi:10.1007/s11214-010-9690-7.

Fejer, B. G., L. Scherliess, and E. R. de Paula (1999), Effects of the vertical plasma drift velocity on the generation and evolution of equatorial spread F, *J. Geophys. Res.*, 104, 19,859–19,869, doi:10.1029/1999JA900025.

Forte, B. (2008), Refractive scattering evidence from multifrequency scintillation spectra observed at auroral latitudes, *Radio Sci.*, 43, RS2012, doi:10.1029/2007RS003715.

Groves, K. M., et al. (1997), Equatorial scintillation and systems support, *Radio Sci.*, 32, 2047–2064, doi:10.1029/97RS00836.

Hajra, R., S. K. Chakraorty, S. Mazumdar, and S. Alex (2012), Evolution of equatorial irregularities under varying electrodynamical conditions: A multi-technique case study from Indian longitude zone, *J. Geophys. Res.*, 117, A08331, doi:10.1029/2012JA017808.

Huba, J. D., A. B. Hassam, I. B. Schwartz, and M. J. Keskinen (1985), Ionospheric turbulence: Interchange instabilities and chaotic fluid behavior, *Geophys. Res. Lett.*, 12, 65–68, doi:10.1029/GL012i001p00065.

Kakad, B., C. K. Nayak, and A. Bhattacharyya (2012), Power spectral characteristics of ESF irregularities during magnetically quiet and disturbed days, *J. Atmos. Sol. Terr. Phys.*, 81, 41–49, doi:10.1016/j.jastp.2012.04.008.

Kakad, B., P. Gurram, P. N. B. Tripura Sundari, and A. Bhattacharyya (2016), Structuring of intermediate scale equatorial spread F irregularities during intense geomagnetic storm of solar cycle 24, *J. Geophys. Res. Space Physics*, 121, 7001–7012, doi:10.1002/2016JA022635.

Lühr, H., C. Xiong, J. Park, and J. Rauberg (2014), Systematic study of intermediate-scale structures of equatorial plasma irregularities in the ionosphere based on CHAMP observations, *Front. Phys.*, 2, 15, doi:10.3389/fphy.2014.00015.

Mullen, J. P., E. Mackenzie, S. Basu, and H. Whitney (1985), UHF/GHz scintillation observed at Ascension Island from 1980 through 1982, *Radio Sci.*, 20, 357–365, doi:10.1029/RS020i003p00357.

Nishioka, M., S. Basu, S. Basu, C. E. Valladares, R. E. Sheehan, P. A. Roddy, and K. M. Groves (2011), C/NOFS satellite observations of equatorial ionospheric plasma structures supported by multiple ground-based diagnostics in October 2008, *J. Geophys. Res.*, *116*, A10323, doi:10.1029/2011JA016446.

Ramsingh, S., S. Sripathi, S. Sreekumar, K. Banola, P. T. Emperumal, and B. S. Kumar (2015), Low-latitude ionosphere response to super geomagnetic storm of 17/18 March 2015: Results from a chain of ground-based observations over Indian sector, *J. Geophys. Res. Space Physics*, *120*, 10,864–10,882, doi:10.1002/2015JA021509.

Redmon, R. J., D. Anderson, R. Caton, and T. Bullett (2010), A Forecasting Ionospheric Real-time Scintillation Tool (FIRST), *Space Weather*, *8*, S12003, doi:10.1029/2010SW000582.

Retterer, J. M. (2010a), Forecasting low-latitude radio scintillation with 3-D ionospheric plume models: 1. Plume model, *J. Geophys. Res.*, *115*, A03306, doi:10.1029/2008JA013839.

Retterer, J. M. (2010b), Forecasting low-latitude radio scintillation with 3-D ionospheric plume models: 2. Scintillation calculation, *J. Geophys. Res.*, *115*, A03307, doi:10.1029/2008JA013840.

Rezende, L. F. C., E. R. de Paula, S. Stephany, I. J. Kantor, M. T. A. H. Muella, P. M. de Siqueira, and K. S. Correa (2010), Survey and prediction of the ionospheric scintillation using data mining techniques, *Space Weather*, *8*, S06D09, doi:10.1029/2009SW000532.

Rino, C. L. (1979), A power law phase screen model for ionospheric scintillation, 2. Strong scatter, *Radio Sci.*, *14*, 1147–1155, doi:10.1029/RS014i006p01147.

Rodrigues, F. S., M. C. Kelley, P. A. Roddy, D. E. Hunton, R. F. Pfaff, O. de La Beaujardière, and G. S. Bust (2009), C/NOFS observations of intermediate and transitional scale-size equatorial spread *F* irregularities, *Geophys. Res. Lett.*, *36*, L00C05, doi:10.1029/2009GL038905.

Sekar, R., and R. Raghavarao (1995), Critical role of the equatorial topside *F* region on the evolutionary characteristics of the plasma bubbles, *Geophys. Res. Lett.*, *22*, 3255–3258, doi:10.1029/95GL03078.

Shkarofsky, I. P. (1968), Generalized turbulence space-correlation and wave-number spectrum function pairs, *Can. J. Phys.*, *46*, 2133–2153, doi:10.1139/p68-562.

Shume, E. B., and D. L. Hysell (2004), Spectral analysis of plasma drift measurements from the AE-E satellite: Evidence of an inertial subrange in equatorial spread *F*, *J. Atmos. Sol. Terr. Phys.*, *66*, 57–65, doi:10.1016/j.jastp.2003.08.005.

Sripathi, S., S. Bose, A. K. Patra, T. K. Pant, B. Kakad, and A. Bhattacharyya (2008), Simultaneous observations of ESF irregularities over Indian region using radar and GPS, *Ann. Geophys.*, *26*, 3197–3213, doi:10.5194/angeo-26-3197-2008.

Sripathi, S., B. Kakad, and A. Bhattacharyya (2011), Study of equinoctial asymmetry in the equatorial spread *F* (ESF) irregularities over Indian region using multi-instrument observations in the descending phase of solar cycle 23, *J. Geophys. Res.*, *116*, A11302, doi:10.1029/2011JA016625.

Sultan, P. J. (1996), Linear theory and modeling of the Rayleigh-Taylor instability leading to the occurrence of equatorial spread *F*, *J. Geophys. Res.*, *101*, 26,875–26,891, doi:10.1029/96JA00682.

Valladares, C. E., J. Villalobos, R. Sheehan, and M. P. Hagan (2004), Latitudinal extension of low-latitude scintillations measured with a network of GPS receivers, *Ann. Geophys.*, *22*, 3155–3175, doi:10.5194/angeo-22-3155-2004.

Whalen, J. A. (2009), The linear dependence of GHz scintillation on electron density observed in the equatorial anomaly, *Ann. Geophys.*, *27*, 1755–1761, doi:10.5194/angeo-27-1755-2009.

Xiong, C., H. Lühr, S. Y. Ma, C. Stolle, and B. G. Fejer (2012), Features of highly structured equatorial plasma irregularities deduced from CHAMP observations, *Ann. Geophys.*, *30*, 1259–1269, doi:10.5194/angeo-30-1259-2012.

Yeh, K. C., and C. H. Liu (1982), Radio wave scintillations in the ionosphere, *Proc. IEEE*, *70*(4), 324–358, doi:10.1109/PROC.1982.12313.

Yokoyama, T., H. Shinagawa, and H. Jin (2014), Nonlinear growth, bifurcation and pinching of equatorial plasma bubble simulated by three-dimensional high-resolution bubble model, *J. Geophys. Res. Space Physics*, *119*, 10,474–10,482, doi:10.1002/2014JA020708.